HAL
open science

Export fluxes of calcite in the eastern equatorial Pacific from the Last Glacial Maximum to present

Paul Loubere, Figen Mekik, Roger Francois, Sylvain Pichat

To cite this version:

Paul Loubere, Figen Mekik, Roger Francois, Sylvain Pichat. Export fluxes of calcite in the eastern equatorial Pacific from the Last Glacial Maximum to present. Paleoceanography, 2004, 19 (2), pp.n/a-n/a. 10.1029/2003PA000986 . hal-02884308

HAL Id: hal-02884308

https://hal.science/hal-02884308v1

Submitted on 31 Jan 2021

HAL is a multi-disciplinary open access archive for the deposit and dissemination of scientific research documents, whether they are published or not. The documents may come from teaching and research institutions in France or abroad, or from public or private research centers.

L'archive ouverte pluridisciplinaire **HAL**, est destinée au dépôt et à la diffusion de documents scientifiques de niveau recherche, publiés ou non, émanant des établissements d'enseignement et de recherche français ou étrangers, des laboratoires publics ou privés.

Export fluxes of calcite in the eastern equatorial Pacific from the Last Glacial Maximum to present

Paul Loubere,[1] Figen Mekik,[2] Roger Francois,[3] and Sylvain Pichat[4,5]

Received 16 November 2003; revised 3 March 2004; accepted 12 April 2004; published 12 June 2004.

[1] The eastern equatorial Pacific (EEP) is an important center of biological productivity, generating significant organic carbon and calcite fluxes to the deep ocean. We reconstructed paleocalcite flux for the past 30,000 years in four cores collected beneath the equatorial upwelling and the South Equatorial Current (SEC) by measuring ex^{230}Th-normalized calcite accumulation rates corrected for dissolution with a newly developed proxy for "fraction of calcite preserved." This method produced very similar results at the four sites and revealed that the export flux of calcite was 30–50% lower during the LGM compared to the Holocene. The internal consistency of these results supports our interpretation, which is also in agreement with emerging data indicating lower glacial productivity in the EEP, possibly as a result of lower nutrient supply from the southern ocean via the Equatorial Undercurrent. However, these findings contradict previous interpretations based on mass accumulation rates (MAR) of biogenic material in the sediment of the EEP, which have been taken as reflecting higher glacial productivity due to stronger wind-driven upwelling. *INDEX TERMS:* 1615 Global Change: Biogeochemical processes (4805); 3030 Marine Geology and Geophysics: Micropaleontology; 4267 Oceanography: General: Paleoceanography; 4805 Oceanography: Biological and Chemical: Biogeochemical cycles (1615); *KEYWORDS:* calcite fluxes, eastern equatorial Pacific, glacial-interglacial

Citation: Loubere, P., F. Mekik, R. Francois, and S. Pichat (2004), Export fluxes of calcite in the eastern equatorial Pacific from the Last Glacial Maximum to present, *Paleoceanography*, *19*, PA2018, doi:10.1029/2003PA000986.

1. Introduction

[2] The tropical Pacific Ocean is a complex environmental system. Winds drive upper ocean circulation, and circulation affects chemical fields and biotic processes. The chemistry and biology are also partially controlled through biogeochemical processes in distant areas, such as the Pacific Subantarctic zone, which is the source region of the lower Equatorial Undercurrent (EUC) [*Toggweiler et al.*, 1991; *Rodgers et al.*, 2003]. The eastern equatorial Pacific (EEP) is the most significant region of CO_2 efflux from the ocean to the atmosphere [*Takahashi et al.*, 2002]. This efflux is mediated by upwelling rates and phytoplankton uptake [*Murray et al.*, 1994]. The latter is apparently Fe limited [*Coale et al.*, 1996], as well as potentially Si limited [*Dugdale and Wilkerson*, 1998; *Dugdale et al.*, 1995; *Wilkerson and Dugdale*, 1996]. Integration of these diverse processes has potential for broad effects on global climate through the marine carbon [*Archer and Maier-Reimer*, 1994; *Matsumoto et al.*, 2002] and nitrogen [*Ganeshram et al.*, 1995, 2000] cycles.

[3] On the basis of an extended history of research on tropical Pacific deep sea sediments, there has developed a general view that the biogeochemical activity of the EEP is mainly controlled by variations in the strength of the trade winds. During glacial intervals the trade winds were thought to be stronger, driving more intense upwelling, increasing the supply of nutrients to the upper ocean, which would have caused higher biological productivity and export to the deep sea (see review in the work of *Loubere* [1999]). Arguments in support of this view were mainly based on estimates of biogenic accumulation rates in the deep sea (calculated using estimated sedimentation rates and dry bulk densities) [e.g., *Lyle et al.*, 1988; *Sarnthein et al.*, 1988; *Pedersen et al.*, 1991] and lower SST at the equator [e.g., *Lyle et al.*, 1992a]. Subsequent geochemical studies suggested that CO_2 concentrations in the upper ocean were higher during glacial periods [*Jasper et al.*, 1994]), nutrient utilization was relatively lower [*Farrell et al.*, 1995] and pH was reduced [*Sanyal et al.*, 1997]. These latter results are not necessarily inconsistent with higher glacial productivity and export but require lower utilization of upwelled nutrients and CO_2, and even higher upwelling rates.

[4] This view of the glacial EEP has been recently challenged in several ways [*Loubere*, 1999]. While it was once thought that reconstructing SST would serve as a proxy of changing upwelling intensity, a number of authors have shown that lateral advection of colder waters from higher southern latitudes via the eastern boundary currents could account for equatorial cooling during glacials [*Lyle et al.*, 1992a, 1992b; *Mix and Morey*, 1996; *Mix et al.*, 1999].

[1]Department of Geology and Environmental Geosciences, Northern Illinois University, DeKalb, Illinois, USA.
[2]Department of Geology, Grand Valley State University, Allendale, Michigan, USA.
[3]Department of Marine Chemistry and Geochemistry, Woods Hole Oceanographic Institution, Woods Hole, Massachusetts, USA.
[4]Laboratoire de Sciences de la Terre, Ecole Normale Superieure de Lyon, Lyon, France.
[5]Now at Department of Earth Sciences, Oxford University, Oxford, UK.

Copyright 2004 by the American Geophysical Union.
0883-8305/04/2003PA000986

The interpretation of glacial SST in the EEP is further obscured as the degree of cooling is controversial [e.g., *Pisias and Mix*, 1997; *Koutavas et al.*, 2002], and glacial planktonic assemblages in the EEP are no-analog [*Mix and Morey*, 1996; *Andreason and Ravelo*, 1997; *Mix et al.*, 1999; *Loubere*, 2001]. So, paleo-SST reconstructions do not unambiguously document past upwelling rates.

[5] Likewise, the notion that glacial productivity in the EEP was uniformly higher is being challenged. Higher concentrations and accumulation rates of organic carbon in sediments have been taken as key indicators for higher glacial productivity [e.g., *Pedersen*, 1983; *Sarnthein et al.*, 1988; *Lyle et al.*, 1988]. However, calculations of biogenic fluxes based on ex^{230}Th (where ex stands for excess) normalization [*Marcantonio et al.*, 2001; *Higgins et al.*, 2002] indicate that the higher glacial accumulation rates could be the result of enhanced sediment focusing (i.e., syndepositional sediment redistribution by bottom currents) rather than increased export flux from surface waters. Beyond this, questions have also arisen concerning the nature of the organic carbon signal, as it is possible that the organic carbon stored in the sediments reflects sources and preservation in addition to biotic flux [e.g., *Keil et al.*, 1994a, 1994b; *Mayer*, 1994a, 1994b; *Loubere*, 1999].

[6] In contrast, tracers of productivity for the EEP that are not based on accumulation rates show lower values for the glacials (e.g., *Wefer et al.* [1990] (Peru margin organic carbon concentration); *Schrader and Sorknes* [1990] (Peru margin diatom assemblages); *Loubere* [1999, 2000, 2002] (benthic foraminiferal transfer function), *Loubere et al.* [2003] (benthic foraminifera, biogenic element ratios); *Ganeshram et al.* [2000] (Peru margin Ba/Al)). Further, synoptic reconstructions based on benthic foraminifera assemblages show that the EEP had a regionally variable productivity response to glacial climate [*Loubere*, 2000, 2002]. While ice age productivity was lower than at present within the Peru upwelling system and the South Equatorial Current (SEC), it appears to have been higher in the Panama Basin and in the lower latitude southern subtropics [*Loubere*, 2002]. These results show lower productivity values for glacial conditions within the region that is directly fed nutrients by upwelling of the lower part of the EUC. These nutrients have their source in the Subantarctic [*Toggweiler et al.*, 1991]. The implication is that changes in EUC chemistry may have been at least as important as the trade winds in governing the biogeochemical behavior of the EEP, and lower glacial age equatorial productivity may have been the result of lower nutrient content in the EUC. This possibility is supported by synoptic mapping of carbon isotope values of the thermocline dwelling planktonic foraminiferal *N. dutertrei* in the EEP [*Loubere*, 2001]. Data for this species indicate that nutrient content of the thermocline was lower during glacials, and that regional gradients, which are pronounced in surface sediments (modern ocean), were much reduced at the LGM. The LGM to modern shift in nutrient content occurred in the early deglacial [*Loubere*, 1999, 2001; *Spero and Lea*, 2002] and seems tied to southern ocean processes.

[7] To further examine changes in EEP biological processes on the glacial-interglacial timescale, and add to our developing picture of organic carbon production outlined above, we present a new method for reconstructing fluxes of biogenic calcite to the seabed. The deep sea record allows us to calculate calcite accumulation rates, but these are difficult to directly interpret in terms of export flux from the overlying surface waters because they are also affected by dissolution at the seabed. Variations in calcite concentration and accumulation observed in the tropical Pacific during the Pleistocene have been ascribed to both changing productivity [e.g., *Arrhenius*, 1952, 1988; *Lyle et al.*, 1988; *Archer*, 1991; *Rea et al.*, 1991; *Weber et al.*, 1995] and preservation [e.g., *Berger*, 1973; *Pisias and Rea*, 1988; *Farrell and Prell*, 1989; *Stephens and Kadko*, 1997]. More recently, *Snoeckx and Rea* [1994] showed that the carbonate patterns of the tropical Pacific are regionally variable, and there is not a uniform tropical Pacific carbonate paleoclimatic signal. In the eastern tropical Pacific, beneath the SEC, *Lyle et al.* [1988, 2002] found calcite accumulation rates during the Last Glacial Maximum that still suggested higher glacial production, notwithstanding improved calcite preservation.

[8] Because sediment fluxes based on excess ^{230}Th normalization have indicated that sediment redistribution can be a problem for the interpretation of mass accumulation rates in the equatorial Pacific [*Paytan et al.*, 1996; *Marcantonio et al.*, 2001; *Higgins et al.*, 2002], we have examined the possible influence of focusing on EEP records by comparing calcite accumulation rates (from sedimentation rates, dry bulk density and calcite concentration) and ex^{230}Th-normalized calcite fluxes. To reconstruct original calcite rain rate to the seafloor, we have divided the ex^{230}Th-normalized records by a new proxy for "fraction of calcite flux preserved" [*Mekik et al.*, 2002], allowing us to determine quantitatively the change in calcite export flux between the LGM and the present. This serves as an independent test of previously made interpretations of paleocalcite production; and sets the stage for regional comparison of organic carbon and calcite flux ratios; changes of which could have significant impact on atmospheric CO_2 content [*Archer and Maier-Reimer*, 1994; *Matsumoto et al.*, 2002].

2. Core Locations and Stratigraphy

[9] Core locations used in this study are shown in Figure 1 (Table 1). In addition to these four cores, we also sampled the core tops from Venture 01-13GC and GS7202-16TW to complete the late Holocene records of ODP846B and RC13-110 respectively. ODP846B and Venture 01-13GC lie under surface waters influenced by the SEC and the upwelling at the Peru margin [*Loubere*, 2000; *Loubere et al.*, 2003] which brings waters originating in the Subantarctic to the mixed layer [*Toggweiler et al.*, 1991]. Y69-71, RC13-110 (GS7202-16) and ODP849B lie progressively westward along the equator and are under the influence of shallow divergence upwelling, which, increasingly westward, draws water from the upper equatorial undercurrent.

[10] Chronologies are based on oxygen isotope stratigraphies and reported in calendar years. Chronologies for ODP846B, Y69-71 and RC13-110 are reviewed in the work of *Loubere et al.* [2003]. ODP846B was originally dated by

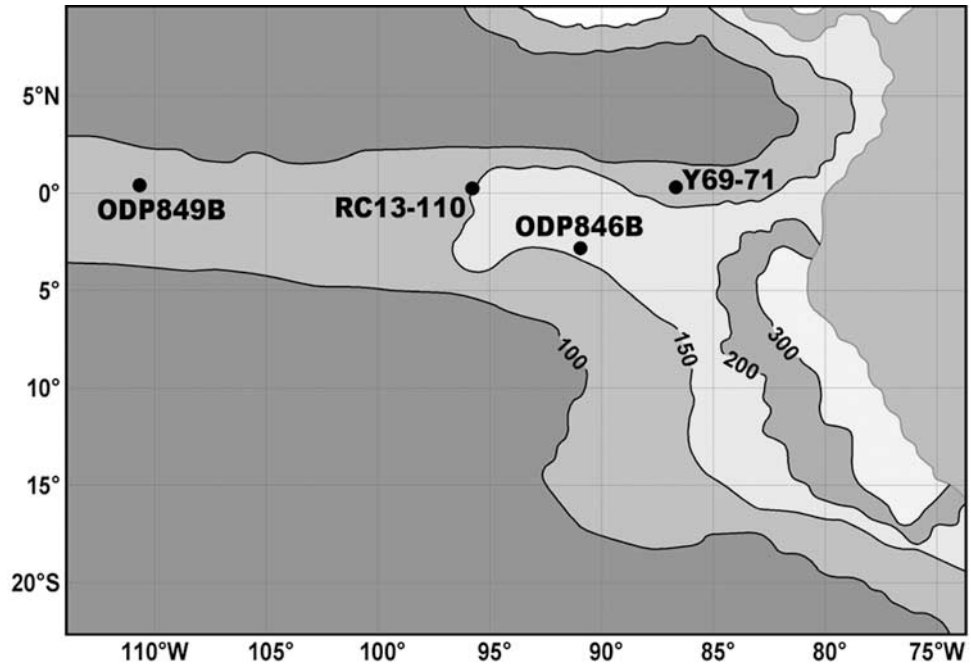

Figure 1. Core locations in the eastern equatorial Pacific. Color gradient represents surface ocean biological productivity after the standard model of *Behrensfeld and Falkowski* [1997]. Contours in gC m^{-2} yr^{-1}. See color version of this figure at back of this issue.

Mix et al. [1995a] and RC13-110 by *Pisias et al.* [1990]. These timescales were slightly modified in the work of *Loubere et al.* [2003] by adjustment to the calendar timescale and by regression of oxygen isotope values against the standard curve of *Martinson et al.* [1987]. Regression was used as a tool to maximize fit (minimize residuals) by adjusting the core timescale to that of the standard for the time period of interest (the last 30,000 years). For Y69-71 the oxygen isotope record was provided by A. Mix (personal communication, 1996) and dating is based on linear interpolation between isotope boundaries. For ODP849B we use the oxygen isotope boundaries and linear interpolations provided by *Mix et al.* [1995b], adjusted for the calendar timescale.

3. Analytical Methods

[11] Data generated for this article include: sediment ex^{230}Th activities (dpm g^{-1}), sediment calcite percent, and estimates of percent calcite flux preserved.

[12] The concentration of ^{230}Th was measured by isotope dilution [*Choi et al.*, 2001] with an inductively coupled plasma mass spectrometer (Finnigan MAT element), after acid digestion of the sediment and Th separation by anion-exchange [*Anderson and Fleer*, 1982]. Precision of the measurement is better than 2%. The accuracy of the analytical method was verified by analyzing samples of Table Mountain Lattite.

[13] Sediment calcite percent was determined using a Carlo-Erba NA1500 C/N/S analyzer, following the methods of *Verardo et al.* [1990]. Samples were calibrated against standard acetanilide and checked against NBS standard reference material 1b (Argillaceous limestone) which has a carbon content of 11.02%. The mean value determined for this standard through replicates (5) run interspersed with the sediments was (11.00%C, s.d. = 0.02%). Replicate analyses of the sediments indicates a mean error of 1.6% calcite (22 replicates).

[14] The percent calcite flux preserved was estimated based on the *G. menardii* fragmentation transfer function of *Mekik et al.* [2002]. For this, an average of 140 *menardii* shells or fragments per sample were counted in ODP846B, 174 in Y69-71, 151 in RC13-110, and 530 in ODP849B. The mean error of the transfer function regression is 5.8% (calibration r^2 = 0.88 for 38 samples). Additionally, there is uncertainty in the scaling of the percent preserved calibration. This uncertainty is estimated to be on the order of 10% [*Mekik et al.*, 2002]. The former is the error estimate for precision, the latter is the potential error in accuracy. The transfer function calibration regression is shown in Figure 2; it is based on gravity core surface sediment samples from the East Pacific Rise and the Ontong-Java plateau.

[15] Percent calcite and dry bulk density (DBD) for Y69-71 and RC13-110 are from *Lyle et al.* [2002]. Dry

Table 1. Core Locations

Core	Latitude	Longitude	Water Depth, m
ODP846B	3.095S	90.818W	3307
Venture01-13MGG	3.09S	90.495W	3304
Y69-71	0.10N	86.48W	2740
RC13-110	0.10N	95.65W	3231
GS7202-16TW	0.07N	98.53W	3183
ODP849B	0.183 N	110.517W	3851

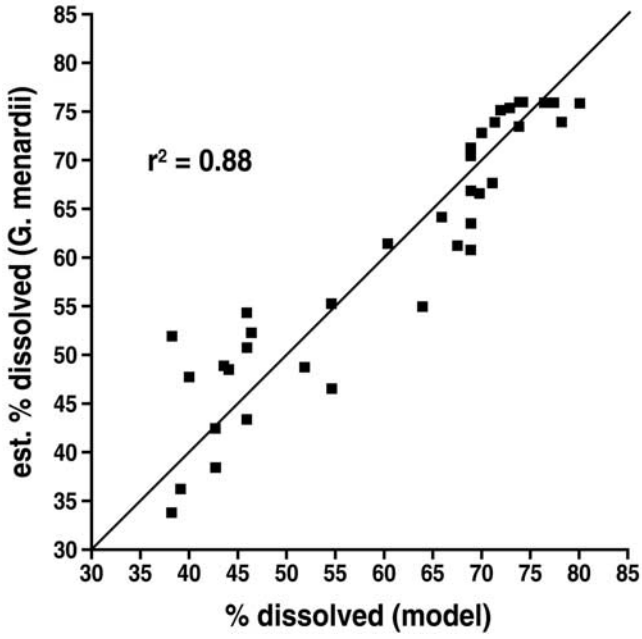

Figure 2. Calibration for the percent dissolved (preserved) proxy based on fragmentation of the planktonic foraminiferal *G. menardii* from *Mekik et al.* [2002]. The calibration was found by regression of a Menardii fragmentation index against model- (Muds) [*Archer et al.*, 2002] derived percent calcite dissolved for surface sediments (gravity cores) from the East Pacific Rise and the Ontong-Java Plateau.

bulk density values for ODP846B and 849B are from data listings in the Ocean Drilling Program [*Pisias and Shipboard Scientific Party*, 1995] with values interpolated to our sampling intervals where necessary. Percent calcite values for Venture 01-13GC are from *Snoeckx and Rea* [1995].

4. Methods for Calculating Sedimentary Calcite Flux

[16] Sedimentary calcite fluxes were obtained (A) by calculating calcite mass accumulation rates (MAR_{carb}) and (B) by normalization to $ex^{230}Th$

MAR calculations :

$$MAR_{carb} = f_{carb}\rho_{dry}(z_2 - z_1)/(t_2 - t_1).$$

[17] Where f_{carb} is the fraction of calcite in the sediments, ρ_{dry} is the dry bulk density of the sediment (g cm^{-3}), z_2 and z_1 are depths of sediment horizons (cm), and t_2 and t_1 are the corresponding sediment ages (kyr), obtained from $\delta^{18}O$ stratigraphy.

[18] This is the more "traditional" method for calculating fluxes from the sedimentary record and the fluxes thus derived are called here "preserved calcite mass accumulation rates." Dividing these estimates by the fraction of calcite preserved provides "original calcite mass accumulation rates."

[19] Because the temporal resolution that can be obtained by this method is inherently limited by the need to take the difference between two measured ages, MARs were calculated for core sections delineated by the most prominent features of their isotope stratigraphy (i.e., postdeglacial; MIS 1/2; MIS 2.2; MIS 2/3). This conservative approach makes our analysis independent of fine tuned age models. Increasing the resolution of the flux record would require dating sediment horizons that are in closer proximity, which automatically would increase the relative error on $(t_2 - t_1)$ and on MAR estimates. Also, variations in f_{carb} between chronological tie points cannot be translated into variations in carbonate flux, since it cannot be ascertained that sediment accumulation rates remain constant over the depth interval considered. In addition to this limitation, traditional MAR estimates also rely on the knowledge of ρ_{dry}, which is another source of error in the calculated fluxes. Perhaps most significantly, MAR estimates do not distinguish between the contribution from vertical fluxes originating from the overlying waters, and lateral fluxes resulting from sediment redistribution by bottom currents. All these problems can, in large part, be resolved by ^{230}Th normalization.

[20] Normalization to $ex^{230}Th$: The ^{230}Th normalization method is detailed in two recent reviews [*Francois et al.*, 2004] and is briefly outlined below.

[21] To clearly distinguish these fluxes obtained by ^{230}Th normalization from those obtained by MAR, we call them "preserved calcite rain rates" to convey the idea that they provide estimates of the vertical flux of calcite originating directly from surface water. Dividing these estimates by the fraction of calcite preserved thus provides "calcite export fluxes."

[22] This method relies on the assumption that the flux of scavenged ^{230}Th reaching the seafloor (F_{230}) is known and equal to the rate of ^{230}Th production from the decay of ^{234}U in the overlying water column (P_{230}) [*Bacon*, 1984; *Suman and Bacon*, 1989; *Francois et al.*, 1990, 2004]:

$$P_{230}\left(\text{dpm m}^{-2}\ \text{yr}^{-1}\right) = \beta_{230}Z = F_{230},$$

where β_{230} is the production rate of ^{230}Th in seawater (0.026 dpm m^{-3} yr^{-1}) and Z is the water depth.

[23] Although only an approximation, this assumption is a priori justified by the very short residence time of ^{230}Th in the water column and its validity has recently been assessed and largely confirmed in modeling [*Henderson et al.*, 1999] and sediment trap [*Yu et al.*, 2001] studies.

[24] With a flux of ^{230}Th scavenged from the water column equal to its known constant rate of production, there is an inverse relationship between the settling material's vertical flux (F_V) and its scavenged ^{230}Th concentration ($[ex^{230}Th]$):

$$\left[ex^{230}Th\right]\left(\text{dpm g}^{-1}\right) = F_{230}\left(\text{dpm m}^{-2}\ \text{yr}^{-1}\right) / F_V\left(\text{g m}^{-2}\ \text{yr}^{-1}\right).$$

[25] Knowing F_{230}, F_V can be calculated from $[ex^{230}Th]$ measured in settling particles. Because of its strong adsorp-

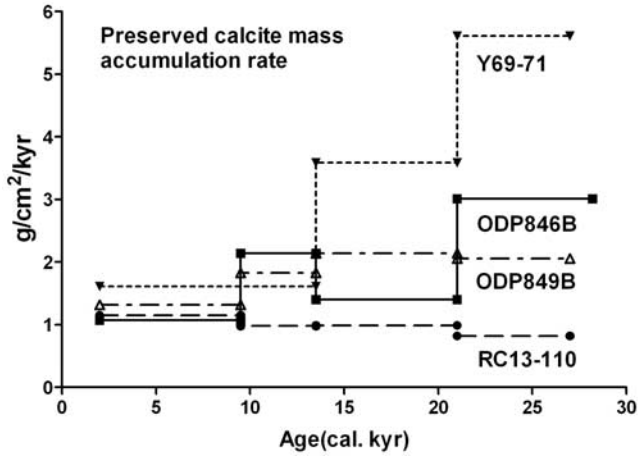

Figure 3. Preserved calcite mass accumulation rates for the four cores based on method A in the text (oxygen isotope stratigraphy combined with dry bulk density measurements). Data in Table 2.

tion properties, scavenged ex^{230}Th remains incorporated into the sediment even after the scavenging particles have been solubilized during early diagenesis, resulting in increased concentration in the accumulating sediment. The fluxes calculated from sediment [ex^{230}Th] are thus "preserved" rain rates ($^{pr}F_V$), i.e., the vertical fluxes of material settling from surface water that remained after diagenetic remineralization. Since ex^{230}Th decays during burial, a correction must also be applied to obtain [ex^{230}Th] at the time of deposition (^{0}[ex^{230}Th]).

$$^{pr}F_V = \beta_{230}\, Z/^{0}[\mathrm{ex}^{230}\mathrm{Th}]$$

"preserved calcite rain rates" can thus be calculated by:

$$[^{pr}F_V]^{carb} = {}^{pr}F_V\ f_{carb}.$$

[26] Because each individual ^{230}Th measurement provides an independent flux estimate, the resolution of the calcite flux reconstruction is not restricted to the resolution of the tie points in the core chronology, as in the MAR method. Also, estimating $^{pr}F_V$ does not require ρ_{dry} to convert linear sedimentation rates to mass accumulation. Finally, to a first order, sediment redistribution does not affect ^{230}Th concentration in sediment, which can still be used to estimate preserved vertical rain rates even in areas of sediment ponding.

5. Results

5.1. Preserved Calcite Accumulation Rates Versus Preserved Calcite Rain Rates

[27] The preserved calcite accumulation rates calculated by traditional means (Figure 3; Table 2) are very different from the preserved rain rates obtained by ^{230}Th normalization (Figure 4; Table 3). Calcite MARs are spatially variable and significantly higher during glacial periods in three of the four cores, especially in eastern cores ODP846B and Y69-71. They are consistent with the results of *Lyle et al.* [2002]. However, the preserved ^{230}Th-normalized rain rates are much lower (by a factor of 2 to 8), differ by less than a factor of two between cores, and do not record highest fluxes at the LGM. Principal components analysis of the preserved rain rates data interpolated at 2 kyr intervals (Table 4; Figure 5) shows that the preserved rain rate record from cores ODP849B, ODP846B and Y69-71 are similar, while that of RC13-110 is significantly different. Principal component 1 accounts for 64% of the data variance and shows a broad peak in accumulation rates between about 10 and 19 kyr. LGM preserved rain rates are higher than those measured for the Late Holocene but lower than those measured during deglaciation in all the cores except RC13-110, which also differs in having maximum preserved rain rate between 8 and 12 kyr.

[28] The much smaller ex^{230}Th-based preserved calcite rain rates indicate that sediment redistribution (focusing) is a significant factor at all coring locations, but particularly for Y69-71. Most notably, the peak in calcite preserved accumulation rates found in the glacial section of three of the four cores (Figure 3) vanishes when applying ex^{230}Th normalization. These higher calcite accumulation rates should thus not be taken as an indication of higher calcite flux from surface water [*Lyle et al.*, 2002]. Instead, our results corroborate those reported by *Marcantonio et al.* [2001] and *Higgins et al.* [2002] and indicate that these higher glacial accumulation rates reflect stronger sediment focusing.

[29] The extent of sediment ponding implied by the ex^{230}Th results can be quantified by the ratio of the traditional calcite accumulation rates to Th-normalized calcite rain rates, or "focusing factor." The latter can also be viewed as the ex^{230}Th accumulation rates normalized to the known production rates of ^{230}Th from ^{234}U decay in the overlying water column [*Suman and Bacon*, 1989]. A focusing factor >1 indicates focusing whereas a focusing factor <1 indicates winnowing. Estimating the ratio requires the selection of time intervals over which ex^{230}Th is averaged. This was done with the same time intervals used for calculating preserved calcite accumulation rates (Figure 6; Table 5). Not surprisingly, the focusing factor of each core share striking similarities with estimates of preserved calcite accumulation rates. The four cores have very different focusing factor (Figure 6) records; although ODP846B and Y69-71 both show markedly higher values for the LGM. The focusing factor at RC13-110 appears to have been nearly constant, and small, over the time interval investigated, while that at ODP849B shows only a modest increase during the glacial. These differences between sites further support the contention that the ex^{230}Th results reflect local sedimentary processes and not regional changes in ex^{230}Th flux to the seafloor between the LGM and the present [*Francois et al.*, 2004].

5.2. Possible Sources of Laterally Redistributed Sediment in the Eastern Equatorial Pacific

[30] An examination of bathymetry for locations where increased LGM calcite accumulation rates have been in-

Table 2. Data for the Calculation of MAR-Based Calcite Accumulation Rates and Paleofluxes[a]

Core	Depth, cm	Age, kyr	Sedimentation Rate, cm kyr^{-1}	Dry Bulk Density	Calcite, %	Age, kyr	Calc. Accumulation, g cm^{-2} kyr^{-1}	Preserved %	Calcite Flux,[b] umol cm^{-2} yr^{-1}
Vent01-13	0	2			60.6	2		15.9	
	5				62.9	3.6		16.8	
ODP846B	6				57.4	5.5		24.4	
	8			0.65					
	12	6.1							
	13				59.1	6.9		31.1	
	19.5				58.4	8.2		32.1	
	23			0.77					
	24	9.5							
Postdeglacial average			2.53	0.71	59.7		1.07	24.06	44.57
	33	12							
	39				60.9	12.9		32.5	
	43	13.5		0.72					
MIS 1/2 interval average			4.87	0.72	60.9		2.14	32.5	65.8
	50				59.8	15		39.4	
	53	15.8							
	59				60.2	17.1		39.8	
	63	18		0.61					
	69				54.3	18		53.3	
	73	21							
MIS 2.2 interval average			3.95	0.61	58.1		1.4	44.6	31.4
	79				58	21.6		45.9	
	83			0.65	54.9	22		41.4	
	88	22.6			54.5	22.6		62.9	
	95				55.6	23.7		43.8	
	100	24.5							
	101				58.5	24.7		56	
	104			0.64					
	107				57.3	25.3		53.7	
	113	25.9			56.4	25.9		51.5	
	119				58.4	26.7		49.3	
	123	27.1		0.62					
MIS 2/3 interval average			8.33	0.64	56.5		3.01	51.2	58.8
	124				52	27.3		47	
	129				51	27.8		42.9	
	133	28.2			51.2	28.2		37.3	
	145			0.6					
Y69-71									
	0	0							
	11		5.4	0.47	60.6	3.5		23.6	
	18		5.4	0.49	62	5		25.9	
	40		5.4	0.51	66.4	7		19.8	
	60		5.4	0.45	58.2	10.6		36.3	
Interval average			5.4	0.48	62.1		1.61	26.4	61
	72.6	13.4	isotope 1/2 boundary						
	79		10.6	0.51	65.7	13.6		32.5	
	99		10.6	0.52	67.6	15.5		39.2	
	121		10.6	0.53	68.5	17.5		42.4	
	140		10.6	0.49	63.8	19		43.1	
Interval average			10.6	0.51	66.4		3.59	39.3	91.3
	153	21	isotope stage 2.2						
	180		16.8	0.5	64.6	22		35.2	
	200		16.8	0.52	66.7	23.5		37.8	
	221		16.8	0.51	66.5	24.8		36	
	241		16.8	0.49	64.1	26.1		48.3	
Interval average			16.8	0.51	65.5		5.61	39.3	142.7
	254	27	isotope 2/3 boundary						
	261		8.7	0.47	61.1	27.8	2.49	34.9	111.7
	532	59							
RC13-110									
	10	3.7		0.53	68.3	3.7		28.3	
	14	4.7							
	20	6.7		0.54	69.8	6.7		35	
	23	7.7							
Interval average			3.1	0.535	69.1		1.15	31.7	36.2
	29	postglacial							
	30	9.9		0.57	71.8	9.9		52.8	
	33	11.8							

Table 2. (continued)

Core	Depth, cm	Age, kyr	Sedimentation Rate, cm kyr^{-1}	Dry Bulk Density	Calcite, %	Age, kyr	Calc. Accumulation, g cm^{-2} kyr^{-1}	Preserved %	Calcite Flux,[b] umol cm^{-2} yr^{-1}
Interval average			2.4	0.57	71.8		0.98	52.8	18.6
	38	MIS 1/2							
	40	14		0.54	69.7	14		44.8	
	43	15.5							
	50	17.3		0.57	72.3	17.3		37.7	
	53	19.2							
Interval average			2.5	0.56	71		0.99	41.3	24.1
	57	MIS 2.2							
	60	22		0.52	66.7	22		37.8	
	63	22.9							
	70	27		0.56	71	27		42.6	
Interval average			2.2	0.54	68.9		0.82	40.2	20.4
	70	MIS 2/3							
	73	27.8							
ODP849B									
	0	0							
	11		3.47	0.55	69	3.4	1.32	26.8	49.3
	33	9.5	end deglacial						
	34		3.84	0.61	77.6	10.3		37.4	
	45		3.84	0.63	75.8	13		37.1	
Interval average			3.84	0.62	76.7		1.83	37.3	49
	48	13.4	isotope 1/2 boundary						
	51		4.21	0.62	76.3	14.5		40.6	
	63		4.21	0.62	83.4	17.2		38.3	
	75		4.21	0.64	81.8	20.2		46.5	
Interval average			4.21	0.63	80.5		2.14	41.8	51.1
	80	21	isotope stage 2.2						
	83		4	0.65	81	22.2	2.11	46.4	
	100		4	0.64	78.7	26	2.01	48.5	
Interval average			4	0.645	79.9		2.06	47.5	43.4
	104	27	isotope 2/3 boundary						
	110		4	0.64	78.9	29.1	2.02	58	34.8

[a]Age dating of sediment intervals is based on oxygen isotope stratigraphy (see text) and identification of 4 intervals, or boundaries: postdeglacial, MIS 1/2, MIS 2.2, and MIS 2/3. Data are averaged for intervals defined by these boundaries for presentation in Figures 3 and 12. See text for data sources.
[b]Here umol cm^{-2} yr^{-1} = 10 × g cm^{-2} kyr^{-1}.

ferred, could help assess the likelihood of lateral transport as a confounding factor. Figure 7 shows core locations and bathymetry in the eastern equatorial Pacific, highlighting cores with higher apparent LGM accumulation rates based on MAR calculations [*Lyle et al.*, 2002]. In all cases the cores are in the vicinity of significant topography. The higher sedimentation rates for these cores could represent downslope sediment transport and not production in the upper ocean. Sediment movement, especially in the fine fraction, from the ridges in the Panama Basin down slope is known to be significant [*van Andel*, 1973].

[31] Further indication of the significance of lateral transport and sediment focusing is provided by comparing the preserved calcite accumulation rate measured in Y69-71 (2740 mbsl) to that measured in a core taken from the top of Carnegie Ridge (V19-27, 1373 mbsl) [*Lyle et al.*, 2002]. Core Y69-71 is important in the EEP since it has the highest sedimentation rates, and focusing factors (Figure 6), of any in the region. Figure 8 shows high-resolution bathymetry of the seafloor from where these two cores were taken. They are both located along the equator and under similar productivity regimes (Figure 1). If anything, production and fluxes should be higher for V19-27. *Lyle et al.* [2002, Figure 3a] show a late Holocene calcite accumulation rate for V19-27 of about 0.8 g cm^{-2} kyr^{-1} and an LGM peak of 2.6 g cm^{-2} kyr^{-1}. For Y69-71 their accumulation rate estimates are 2.2 g cm^{-2} kyr^{-1} for the late Holocene and 5 g cm^{-2} kyr^{-1} for the LGM, which is similar to our estimates (Figure 3). Thus calcite MARs are higher in the deeper core, in spite of the fact that V19-27

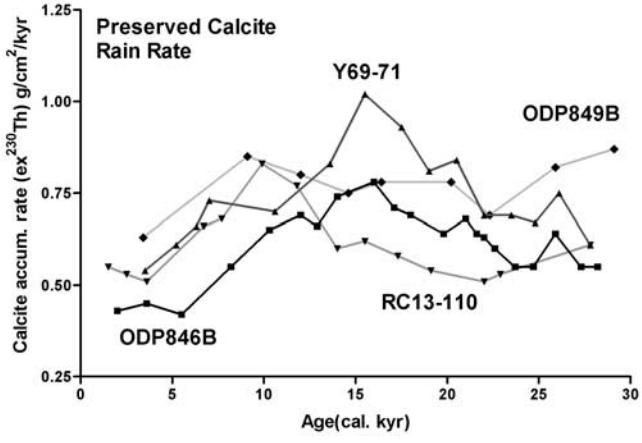

Figure 4. Preserved calcite rain rates for the four cores based on method B in the text (ex^{230}Th normalization). Data in Table 3. See color version of this figure at back of this issue.

Table 3. Data for ex^{230}Th Normalization and Calcite Flux Calculations for the Four Cores[a]

Core	Depth, cm	Age, kyr	ex^{230}Th, dpm g^{-1}	Calcite, %	Calcite Accumulation Rate, g cm^{-2} kyr^{-1}	Preserved %	Count	Calculated Flux,[b] umol cm^{-1} yr^{-1}
Vent01-13	0.0	2.00	12.06	60.60	0.43	15.90	C	26.90
Vent01-13	5.0	3.60	11.69	62.90	0.45	16.80	C	26.70
ODP846B	6.0	5.50	11.33	57.40	0.42	24.40	C	17.20
	13.0			59.10		31.07	C	
	19.5	8.20	8.8	58.40	0.55	32.10		17.10
	27.0	10.30	7.23	T60	0.65	33.70	C	19.20
	33.0	12.00	6.8	T60.5	0.69	33.50	C	20.40
	39.0	12.90	7.08	60.90	0.66	32.50	C	20.00
	43.0					38.30	C	
	45.0	14.00	6.16	T60	0.74	38.30		19.30
	50.0			59.80		39.40	C	
	54.0	16.00	5.79	T60	0.78	44.00	C	17.70
	59.0	17.10	6.26	60.20	0.71	39.80	C	17.80
	63.0	18.00	6.13	T57.8	0.69	57.70	C	11.90
	69.0	19.80	6.1	54.30	0.64	53.30		12.00
	73.0	21.00	5.89	T56.1	0.68	50.40		13.50
	79.0	21.60	6.45	58.00	0.64	45.90	C	13.90
	83.0	22.00	6.2	54.90	0.63	41.40	C	15.20
	88.0	22.60	6.41	54.50	0.6	62.90	C	9.50
	95.0	23.70	7.11	55.60	0.55	43.80	C	12.60
	101.0	24.70	7.4	58.50	0.55	56.00	C	9.80
	107.0			57.30				
	113.0	25.90	5.99	56.00	0.64	51.50		12.40
	119.0			58.40				
	124.0	27.30	6.38	52.00	0.55	47.00	C	11.70
	129.0			51.00		42.90		
	133.0	28.20	6.24	51.20	0.55	37.30	C	14.70
Y69-71P	10.0	3.50	7.8	60.60	0.54	23.60	C	22.90
	18.0					25.90	C	
	20.0	5.20	7.22	63.70	0.61	24.80		24.60
	30.0	6.30	6.71	65.10	0.66	21.30	C	30.90
	40.0	7.00	6.17	66.40	0.73	19.80	C	36.70
	50.0					26.40	C	
	60.0	10.60	5.47	58.20	0.7	36.30	C	19.30
	71.0					29.30	C	
	80.0	13.60	5.04	65.70	0.83	32.50		25.50
	90.0					36.80	C	
	100.0	15.50	4.14	67.60	1.02	39.20	C	26.00
	112.0					43.10	C	
	120.0	17.50	4.52	68.50	0.93	42.40	C	21.90
	130.0					32.30	C	
	139.0	19.00	4.79	63.80	0.81	43.10		18.80
	146.0					49.50	C	
	160.0	20.50	4.58	64.20	0.84	44.30		18.90
	170.0					40.60	C	
	180.0	22.00	5.51	64.60	0.69	35.20		19.60
	200.0	23.50	5.59	66.70	0.69	37.80	C	18.20
	220.0	24.80	5.65	66.50	0.67	36.00	C	18.60
	240.0	26.10	4.87	64.10	0.75	48.30	C	15.50
	260.0	27.80	5.58	61.10	0.61	34.90	C	17.50
GS720216	0.0	1.50	10.6	70.80	0.55	26.50	C	20.70
RC13-110	5.0	2.50	9.8	62.70	0.53	27.40		19.30
	10.0	3.60	11.02	68.30	0.51	28.30	C	17.90
	14.0					29.90	C	
	20.0	6.70	8.42	69.80	0.66	35.00	C	18.90
	23.0	7.70	8.31	71.20	0.68	40.50	C	16.80
	30.0	9.90	6.75	71.80	0.83	52.80	C	15.60
	33.0	11.80	7.05	71.60	0.77	52.40	C	14.70
	40.0	14.00	8.72	69.70	0.6	44.80	C	13.40
	43.0	15.50	8.31	70.20	0.62	48.00	C	12.90
	50.0	17.30	9.02	72.30	0.58	37.70	C	15.40
	53.0	19.10	9.26	70.60	0.54	37.30	C	14.50
	60.0	22.00	9.02	66.70	0.51	37.80	C	13.50
	63.0	22.90	8.83	67.90	0.53	39.90	C	13.30
	70.0					42.60	C	
	73.0	27.80	7.8	69.70	0.61	36.40	C	16.70
ODP849B	11.0	3.40	10.67	69.00	0.63	26.80	C	23.60
	30.0	9.10	8.3	76.00	0.85	35.00		24.20
	34.0			77.60		37.40	C	

Table 3. (continued)

Core	Depth, cm	Age, kyr	ex^{230}Th, dpm g^{-1}	Calcite, %	Calcite Accumulation Rate, g cm^{-2} kyr^{-1}	Preserved %	Count	Calculated Flux,[b] umol cm^{-1} yr^{-1}
	40.0	12.00	8.4	T76.5	0.8	37.20		22.00
	45.0			75.80		37.10	C	
	51.0	14.60	8.87	76.30	0.75	40.60	C	18.50
	61.0	16.40	9.21	T82	0.78	39.00		20.00
	63.0			83.40		38.30	C	
	75.0	20.20	8.48	81.80	0.78	46.50	C	16.80
	83.0	22.30	9.31	81.00	0.69	46.40	C	14.90
	100.0	25.90	7.24	78.70	0.82	48.50	C	16.90
	110.0	29.10	6.69	78.90	0.87	58.00	C	15.00
	120.0	31.70	6.08	T79	0.94	61.00		15.40
	123.0			79.00		63.70	C	

[a]See Table 1. Here T = interpolated value and C = G. menardii count done.
[b]Here umol cm^{-2} yr^{-1} = g cm^{-2} kyr^{-1} × 10.

is above, and Y69-71 is within, the calcite lysocline for the EEP. Taking into account higher dissolution for the deeper site, the supply of calcite to the Y69-71 location must have been considerably higher than at the V19-27 site even though surface ocean production is unlikely to be different.

[32] We can quantify the vertical calcite supply rate that would be required to sustain the measured accumulation rates in the two cores using *Archer et al.*'s [2002] Muds calcite diagenesis model. We used present-day bottom water physical/chemical conditions [*Archer*, 1996; D. Archer, personal communication, 2000] and estimates of surface ocean biological production [*Behrenfeld and Falkowski*, 1997] converted to seabed fluxes [*Berger et al.*, 1989]. We found that calcite accumulation rates at Y69-71 should be 50 to 75% of those at V19-27 if calcite and organic carbon export fluxes were the same at the two sites and if sediment passively accumulated on the seabed. Since we observe the opposite (i.e., calcite MARs are ~3 times higher in Y69-71), these modeling results support our inference that a substantial portion of the calcite accumulation at Y69-71 comes from lateral sources.

[33] An examination of the multibeam image in Figure 8a shows that Y69-71 is within a basin surrounded on three sides by elevations. Given the winnowing that is occurring across the higher bathymetry, it is not surprising that this location should see an influx of laterally transported sediment. In fact, thorium normalization indicates that more than half of the modern sediment flux is from such transport. Sediment trap observations by *Honjo et al.* [1982] show that lateral supply of sediment is a significant feature in deep waters of the Panama Basin.

[34] *Lyle et al.* [2002] also report higher calcite MAR during the LGM in V19-27, which they point to as further evidence for increased calcite export during that time. We do not have ^{230}Th data from this core to address this question thoroughly, but we note however, that V19-27 is also located in a setting that could be compromised by seabed transport processes, enhancing either winnowing or focusing. Figure 8b indicates that the coring site is on the flank of a high along the Carnegie Ridge, and is near the head of a canyon system feeding the abyssal plain to the north. The potential complexity of the sedimentation regime at this location is indicated by the calcium carbonate concentration which varies from about 33% during late Holocene to nearly 75% in the deglacial/MIS2-3 interval (shown in the work of *Lyle et al.* [2002]), which is not seen in any other core in the EEP. Examination of Figures 7 and 8 indicates that finding locations free of lateral sediment transport in the EEP would be difficult. Interpretation of

Table 4. Principal Components Analysis of Calcite Accumulation Rate and Calcite Flux (230-Th-normalized) for the Four Cores

Core	Correlation of Core Record: Accumulation Rate PC1	Correlation of Core Record: Flux PC1
ODP846	0.9000	0.8266
Y69-71	0.8635	0.7329
RC13-110	0.5025	0.8194
ODP849	0.8714	0.9585
Variance Explained, %	64.2	70.3

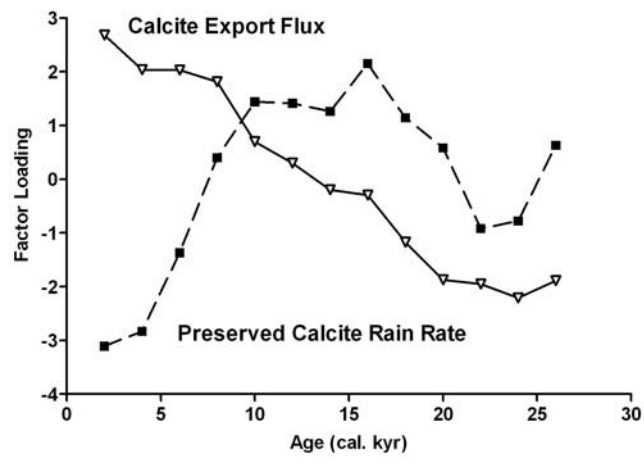

Figure 5. First principal component for preserved calcite rain rates and calcite export fluxes for the four cores. Cores were analyzed by interpolating values at 2000 year intervals in each record.

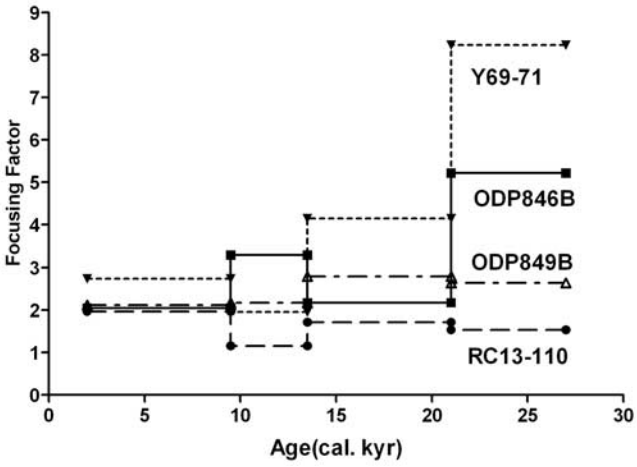

Figure 6. Ratio of preserved calcite MAR over ex^{230}Th-normalized fluxes, or focusing factor, for the four cores. Data in Table 5.

accumulation rate data would seem to demand a proxy such as ex^{230}Th to provide for normalization in the face of widespread sediment redistribution at the seabed.

5.3. Reconstruction of Calcite Preservation in the EEP

[35] Reconstruction of down core percent calcite preserved is shown in Figure 9. All the cores show a trend of decreasing preservation from the LGM to the present, confirming that lower Holocene carbonate accumulation rate in the sediment of the EEP is mainly driven by increased dissolution [*Berger*, 1973; *Pisias and Rea*, 1988; *Farrell and Prell*, 1989; *Stephens and Kadko*, 1997]. We find lowest preservation in surface sediment samples, which is in accord with other evidence for enhanced dissolution in the sediment recently deposited in the deep Pacific [*Berelson et al.*, 1997]. Calcite preservation in ODP846B, ODP 849B and Y69-71 is similar. It is highest prior to 15ka BP and gradually decreases toward the present. In core RC13-110, preservation follows a distinct trend with only a modest difference between the LGM and present (at most 10%; Table 3), and a prominent preservation peak in the early Holocene.

[36] Considering the different mass accumulation rates characterizing Y69-71 and the two ODP cores, the similarity in calcite preservation that we find in these three cores is puzzling. Higher calcite accumulation rate should enhance preservation and we might expect to find higher preservation in Y69-71, particularly during the LGM. In order to evaluate whether such an effect would be distinguishable within the errors of our analysis, we used the Muds model [*Archer et al.*, 2002] to calculate carbonate preservation as a function of accumulation rates, under modern deep-water conditions (Tables 6a–6d). The model was run under two regimes. In the first regime, the fluxes of organic carbon, opal and clays were gradually increased, while calcite fluxes were adjusted so that sediment percent calcite remained constant. This mimics a shift to higher surface ocean production of organic carbon and calcite combined with a proportional increase in opal/clay sedimentation, and the observation (Tables 6a–6d) that Holocene and LGM sediment percent calcite are similar for our sites. It should be noted that the percent calcite constraint meant that as sediment flux was increased, the organic carbon to calcite flux ratio also increased. In the second regime, the model was run as if increased flux was due to water column funneling or syndepositional sediment redistribution to a

Table 5. Comparison of Traditional and ex Th Methods for Calculation of Sediment Accumulation Rates and the Focusing Factor as a Ratio of the Methods[a]

Age Interval, kyr	Sediment Interval, cm	Sediment Rate, cm kyr^{-1}	DBD, G cm^{-3}	Accumulation Rate, g cm^{-2} kyr^{-1}	^{230}Th Accumulation, g cm^{-2} kyr^{-1}	Focusing Factor
			ODP846B			
0–9.5	0–24	2.53	0.65	1.64	0.8	2.05
9.5–13.4	24–43	4.87	0.74	3.6	1.09	3.3
13.4–21	43–73	3.95	0.66	2.61	1.2	2.18
21–27	73–123	8.33	0.64	5.33	1.02	5.22
			Y69-71			
0–9.5	0–54	5.7	0.49	2.79	1.02	2.74
9.5–13.4	54–73	4.9	0.48	2.35	1.2	1.96
13.4–21	73–153	10.5	0.51	5.36	1.29	4.15
21–27	153–254	16.8	0.5	8.4	1.02	8.24
			RC13-110			
0–9.5	0–29	3.1	0.54	1.67	0.85	1.97
9.5–13.4	29–38	2.3	0.56	1.29	1.11	1.16
13.4–21	38–57	2.5	0.55	1.38	0.8	1.72
21–27	57–70	2.2	0.54	1.19	0.77	1.54
			ODP849B			
0–9.5	0–33	3.5	0.55	1.93	0.91	2.12
9.5–13.4	33–48	3.8	0.62	2.36	1.08	2.18
13.4–21	48–80	4.2	0.62	2.6	0.93	2.8
21–27	80–104	4	0.64	2.56	0.97	2.64

[a]Age intervals are: 9.5 kyr = base of Holocene; 13.4 kyr = MIS 1/2 boundary; 21 kyr = MIS 2.2; 27 kyr = MIS 2/3 boundary.

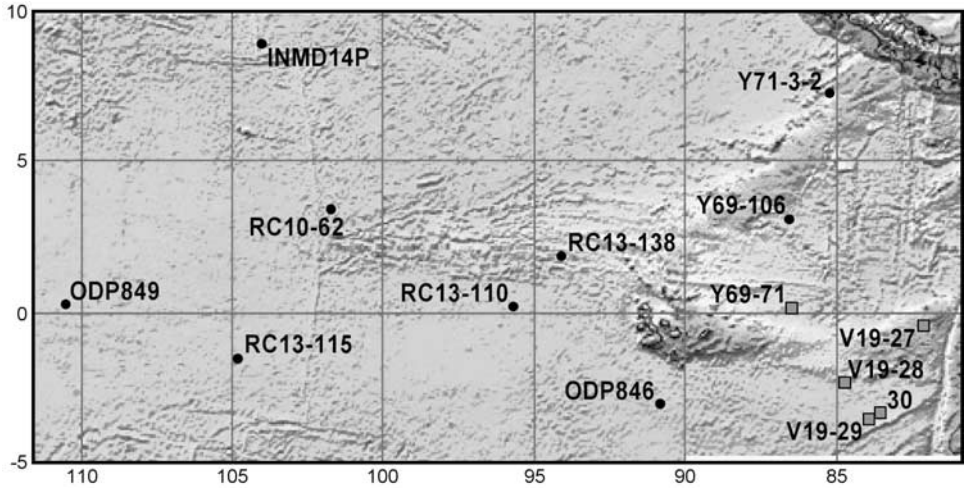

Figure 7. Core locations for this study and *Lyle et al.* [2002] used for calcite accumulation rate determinations, plotted on bathymetry from *Smith and Sandwell* [1997]. Locations marked by squares are those showing elevated LGM preserved calcite mass accumulation rates. See color version of this figure at back of this issue.

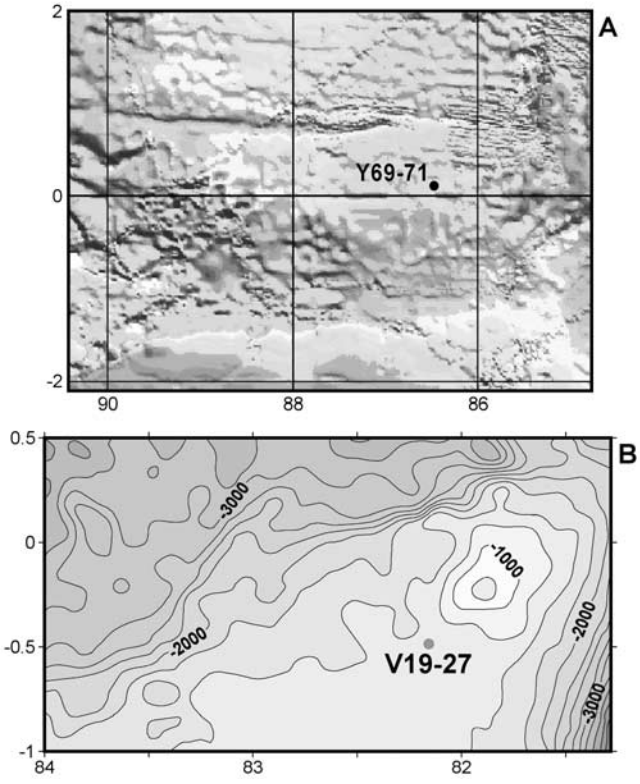

Figure 8. (a) Location of Y69-71 on multibeam bathymetry from the RIDGE Web site (http://ocean-ridge.ldeo.columbia.edu/general/html/RMBS-intro.html; http://ocean-ridge.ldeo.columbia.edu/database/html/home.html). (b) Location of V19-27 on bathymetry from *Smith and Sandwell* [1997]; see http://topex.ucsd.edu/marine_topo/mar_topo.html. See color version of this figure at back of this issue.

spot on the ocean floor. In this case, sediment percent calcite was allowed to vary while the flux ratios of sediment components were held constant.

[37] In both regimes, the model predicted that a three fold increase in calcite accumulation rates should lead to an increase in calcite percent preserved between 10 and 20%. Since Glacial accumulation rates in core Y69-71 are about 3 times higher than in the ODP cores, model results indicate that this should have resulted in a discernible increase in preservation in Y69-71, which we do not observe (Figure 9). Thus these results do not meet expectations if changes in accumulation rates were due to changes in rain rate from the overlying surface water [*Lyle et al.*, 2002], changes in water column "funneling" or instantaneous redistribution of sediment on the seafloor. We are therefore left with the expla-

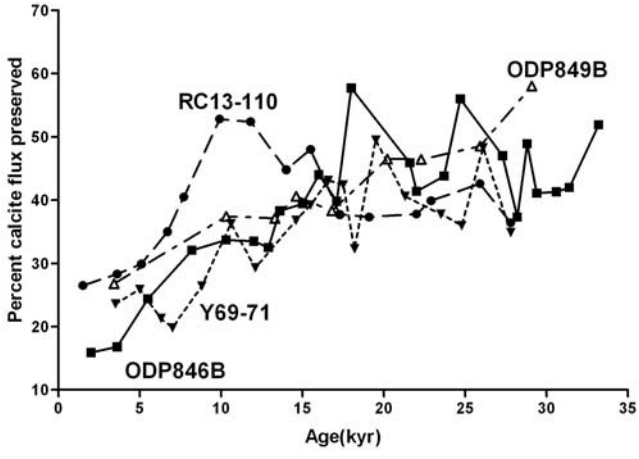

Figure 9. Calcite percent preserved for the four cores; see text for methods. Data in Table 3.

Table 6a. Modeling Results for Effect of Increasing Sediment Accumulation Rate on Percent Calcite Preserved: Modeling Using Modern Conditions for ODP846B and With Percent Calcite in the Sediments Fixed[a]

Factor Increase in Noncarbonate Component Rain	Calculated Rain of Calcite, umol cm^{-2} yr^{-1}	Dissolution Rate, umol cm^{-2} yr^{-1}	Calcite Accumulation Rate, umol cm^{-2} yr^{-1}	Calcite Preserved, %	Sediment Accumulation Rate, umol cm^{-2} yr^{-1}	Sediment Accumulation Rate Increase Factor
1.0	21.4	−17.0	4.4	21.0	7.2	1.0
1.5	28.0	−21.4	6.7	23.9	10.98	1.53
2.0	34.1	−25.0	9.1	26.7	14.92	2.07
2.5	39.0	−27.3	11.7	30.0	19.18	2.7
3.0	43.5	−29.2	14.3	32.8	23.44	3.25
4.0	53.8	−34.1	19.7	36.6	32.3	4.49
6.0	72.6	−41.3	31.3	43.1	51.31	7.13

[a]Here flux ratio variable so that sediment calcite percent = 61. Model parameters are as follows: water depth, 3307 m; T, 1.5C; Sal, 34.7SU; alkalinity, 2779 umol kg^{-1}; O2, 130 umol kg^{-1}; delta calcite, −15 umol; organic carbon flux, 21 umol cm^{-2} yr^{-1}; clay/opal accumulation rate, 273 ug cm^{-2} yr^{-1}; and sediment percent calcite, 61. Basic chemical and physical values from *NOAA* [1994], alkalinity from *Archer* [1996] and D. Archer (personal communication, 2000) rates from thorium normalization, and organic carbon flux from transformation of surface production estimates (standard model) [*Behrenfeld and Falkowski*, 1997] converted to seabed flux [*Berger et al.*, 1989].

nation that changes in MAR are driven by "delayed" focusing, with calcite dissolution occurring mostly during postdepositional lateral transport to the final burial site. The dissolution index would thus acquire a "regional" preservation signal which would be minimally impacted by site-specific accumulation rates. This scenario offers the simplest explanation for the uniformity of the calcite preservation records (Figure 9) that we have found for the four cores we examined, in spite of their very different focusing/MAR histories.

[38] Our results imply quite significant transport of sediments on the seafloor. This transportation process is not well known, and its impact on proxies obviously needs better understanding. In particular, it might influence our estimates of calcite preservation by differentially transporting *G. menardii* particles. By increasing the relative abundance of finer particles, sediment focusing could bias the MFI index toward lower preservation estimates. In reality, however, the MFI index is based on sand sized particles (>150 um fraction) that consist of whole shell and damaged shells, which probably do not differ much in hydrodynamic properties. Also, Figure 10 shows the preservation and sediment focusing records of ODP846B, the site where we have the most data. The two are not similar. Sediment focusing decreases markedly from an LGM high at about 20 kyr BP and stays relatively constant while percent preserved remains high until 15 kyr BP and decreases gradually. This result indicates that sediment focusing has not significantly biased the percent preserved proxy. Since we do not find lower preservation in the glacial section of Y69-71 compared to the two ODP cores, we conclude that particle sorting has little effect on our estimate of percent preservation.

[39] Because the two focusing-related effects on preservation are opposite, there is also the possibility that both enhanced preservation due to higher accumulation rate and lower apparent preservation due to sorting could fortuitously cancel each other so that the preservation profiles of the 4 cores are made similar. If that were the case, we would increasingly underestimate the true degree of calcite preservation as sediment focusing increases (i.e., preservation would indeed be better in cores with higher focusing but sorting would bias the MFI index just in the exact proportion to negate this effect). Sediment transport remains an under-explored potential bias in paleoceanic proxies, and it is hard to estimate how much error it might impose on our results. However, we take the improbability that the two effects would cancel each other exactly at the

Table 6b. Modeling Results for Effect of Increasing Sediment Accumulation Rate on Percent Calcite Preserved: Modeling Using Modern Conditions for ODP846B Keeping All Flux Ratios Constant, Allowing Sediment Percent Calcite to Vary[a]

Focusing Factor Equivalent	Calcite Accumulation Rate, umol cm^{-2} yr^{-1}	Sediment Accumulation Rate, umol cm^{-2} yr^{-1}	Calcite in Sediments, %	Calcite Preserved, %	Sediment Accumulation Rate Increase Factor
1.0	4.4	7.2	61.0	21.0	1.0
1.5	9.9	14.1	70	31.2	1.96
2	16.1	21.9	73.4	38.1	3.04
2.5	23.9	31.4	76.1	45.4	4.4
3	32.5	41.9	77.6	51.2	5.8

[a]Here a constant flux ratio was used. Model parameters are as follows: water depth, 3307 m; T, 1.5C; Sal, 34.7SU; alkalinity, 2779 umol kg^{-1}; O2, 130 umol kg^{-1}; delta calcite, −15 umol; organic carbon flux, 21 umol cm^{-2} yr^{-1}; clay/opal accumulation rate, 273 ug cm^{-2} yr^{-1}; and sediment percent calcite, 61. Basic chemical and physical values from *NOAA* [1994], alkalinity from *Archer* [1996] and D. Archer (personal communication, 2000) rates from thorium normalization, and organic carbon flux from transformation of surface production estimates (standard model) [*Behrenfeld and Falkowski*, 1997] converted to seabed flux [*Berger et al.*, 1989].

Table 6c. Modeling Results for Effect of Increasing Sediment Accumulation Rate on Percent Calcite Preserved: Percent Calcite and Percent Preserved as Observed in the Four Cores Analyzed

Site	Holocene Focusing Factor	LGM Focusing Factor	Holocene Preserved, %	LGM Preserved, %	Holocene Calcite, %	LGM Calcite, %
ODP846	2	5	15–20	45–55	61	57
Y69-71	3	8	20–25	40–45	61	64
RC13-110	2	1.5	20–25	35–40	70	67
ODP849	2	2.5	25–30	45–50	69	81

four sites, as an indication that sediment focusing minimally affects our estimates of carbonate preservation. This is further supported by the spatial coherence that we observe in our reconstruction of calcite export at the four sites (see below). Only additional reconstructions within the EEP could confirm this conclusion.

5.4. Reconstruction of Calcite Export From the Overlying Surface Water of the EEP

[40] The export fluxes of calcite from surface waters (Figure 11) were produced by dividing the ex^{230}Th-based preserved calcite rain rates (Figure 4) by the fraction of calcite preserved (Figure 9). The results are quite similar at the four sites. The highest calcite export fluxes are found during the latest Holocene, while LGM fluxes were significantly lower. Glacial export fluxes may have been particularly low at site ODP846B, which is within the EEP most under the influence of the Peru upwelling system (Figure 1).

[41] Results for calcite export are summarized by principal components analysis in Figure 5 and Table 4. The first principal component accounts for 70% of data variance and all 4 cores correlate strongly to it. Hence application of the percent preserved proxy further improves the correspondence among the cores which was already observed for the ^{230}Th-based rain rates (Figure 4).

[42] The results indicate a broad pattern of calcite flux response across the region of the EEP supplied in nutrients by upwelling of water transported by the EUC. The flux began to increase, following the LGM low, at about 17 kyr and reached peak values after 10 kyr.

[43] Table 7 presents an estimate of the present to LGM change in calcite flux for the two cores for which we have surface sediment (modern) data. The estimates indicate the LGM flux was between a third and one-half lower than the modern. Table 7 also presents minimal estimates of the present-LGM difference. This was calculated by shifting the modern and LGM percent calcite preserved values by the standard error in such a way as to minimize the flux difference. This analysis indicates that the present-LGM calcite flux difference was at least greater than 10 to 20%.

[44] Reconstruction of paleocalcite flux using the traditionally calculated calcite accumulation rates is shown in Figure 12. The fluxes calculated here are much higher than those based on ex^{230}Th normalization. *Archer* [1996] shows that highest EEP calcite export fluxes,

Table 6d. Modeling Results for Effect of Increasing Sediment Accumulation Rate on Percent Calcite Preserved: Size Fraction Weight Percent in Holocene and LGM Sediments of ODP846B

Depth, cm	Age, kyr	Percent > 63 um	Percent > 150 um
6	5.5	22.2	12.4
14	7.3	18	10.5
40	13	19.8	14.7
80	21.6	19	11.7
84	22	19.8	12.6
89	22.6	18	
96	23.8	16.6	9.7

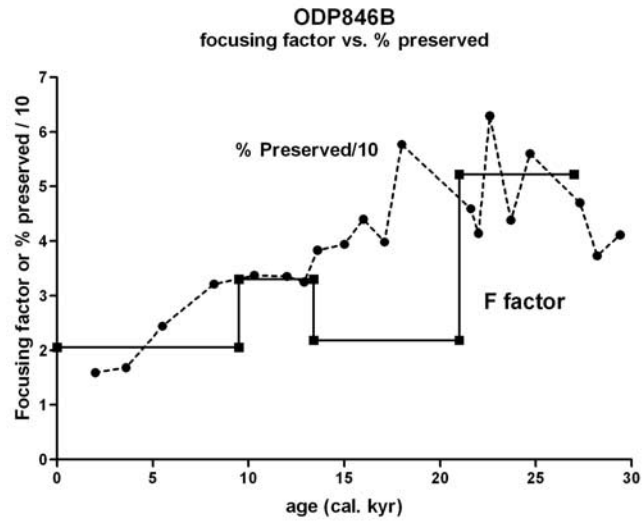

Figure 10. Calcite percent preserved plotted against sediment focusing factor for ODP846B.

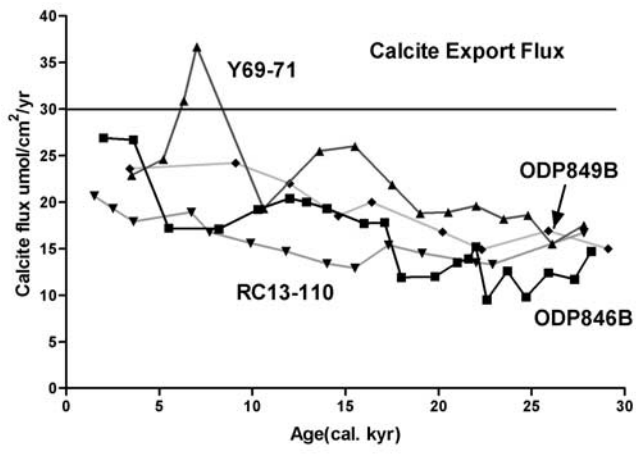

Figure 11. Calcite export flux calculated for the four cores found by dividing the ex^{230}Th accumulation rates by fraction calcite preserved. Note that umol cm^{-2} yr^{-1} = 10 × g cm^{-2} kyr^{-1}. See color version of this figure at back of this issue.

both by sediment trap data and modeling, are about 30 umol cm^{-2} yr^{-1} for the modern. This is exceeded by the late Holocene MAR method values of all the cores, especially in Y69-71 where the Holocene flux is 61 umol cm^{-2} yr^{-1}. By contrast, the $ex^{230}Th$-normalized fluxes (Figure 11) for the late Holocene are between 20 and 30 umol cm^{-2} yr^{-1} in the four cores, and closer to those expected from the literature.

[45] The down core variations in the original calcite MAR are different in the four cores, with Y69-71 showing a very high LGM to present shift (by a factor greater than 2). The LGM to present decrease is less dramatic for ODP846B (59 to 41 umol cm^{-2} yr^{-1}). RC13-110 and 849B show a modest LGM to present difference with LGM fluxes somewhat lower than the modern. The dissimilarity of these results contrasts with those obtained using $ex^{230}Th$ normalization, further indicating that location specific seabed factors have influenced sediment accumulation.

6. Conclusions

[46] Our results add further evidence that seabed accumulation of biogenic sediments in some regions of the tropical Pacific can be seriously influenced by syndepositional sediment redistribution. The effect is dependent on location, but appears to have been enhanced at several of our locations during the Last Glacial Maximum. Because of this, accumulation rates calculated between dated sediment horizons cannot be interpreted simply in terms of surface ocean production. Normalization to a constant accumulation rate tracer such as $ex^{230}Th$ is necessary to reconstruct past biogenic rain rates originating from overlying surface waters.

[47] Normalizing calcite flux to $ex^{230}Th$ in the eastern equatorial Pacific yields rain rate profiles very different from accumulation rates. Correcting the $ex^{230}Th$-normalized calcite rain rates with a proxy for " percent calcite preserved" reveals a fairly simple and consistent picture of LGM to present change in calcite export fluxes in the equatorial upwelling and SEC section of the EEP. In this region, the LGM calcite export flux was lower than at present by about 30–50%. Calcite fluxes began to rise early during deglaciation, following a pattern consistent with previous observations that deglacial response in the tropical Pacific follows southern ocean timing [*Loubere*, 1999, 2001; *Spero and Lea*, 2002; *Loubere et al.*, 2003]. This timing matches that of other biogeochemical proxies in the EEP [*Loubere*, 2001; *Spero and Lea*, 2002].

[48] The trend reconstructed by 230Th normalization is opposite to that deduced from MAR measurements in earlier studies [e.g., *Arrhenius*, 1952; *Sarnthein et al.*, 1988; *Lyle et al.*, 1988, 2002], but in agreement with paleoproductivity tracers showing lowered values for the LGM [*Stephens and Kadko*, 1997; *Wefer et al.*, 1990; *Schrader and Sorknes*, 1990; *Loubere*, 1999, 2000; *Ganeshram et al.*, 2000; *Loubere et al.*, 2003; S. Pichat et al., Lower biological productivity during glacial periods in the equatorial Pacific as derived from $(^{231}Pa/^{230}Th)_{xs,0}$ measurements in deep-sea sediments, submitted to *Paleoceanography*, 2004] along the Peru margin and in the equatorial upwelling band of the EEP. Unlike the calcite export fluxes based on ^{230}Th normalization, those based on MAR are variable between sites and result in modern calcite fluxes that are significantly higher than the best estimates based on sediment traps and modeling.

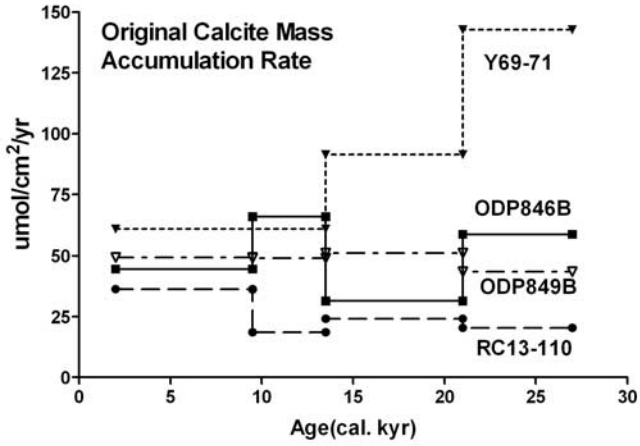

Figure 12. Original calcite mass accumulation rates calculated for the four cores found by dividing the preserved calcite mass accumulation rates by fraction calcite preserved. Note that umol cm^{-2} yr^{-1} = 10 × g cm^{-2} kyr^{-2}.

Table 7. Present to LGM Calcite Flux Difference for Cores With Surface Sediment Data Available[a]

Core	Age	Samples	Preserved, %	Calcite Flux, umol cm^{-2} yr^{-1}	Difference, umol cm^{-2} yr^{-1}	Difference, %
Modern to LGM Calcite Flux Difference Estimate; Data in Table 3						
ODP846B	surface	1	15.9	26.9		
					12.7	47
	21–22 kyr	3	45.9	14.2		
RC13-110	surface	1	26.5	20.7		
					7.3	35
	21–23 kyr	2	38.9	13.4		
Minimal Difference Estimate						
ODP846B	surface	1	21.7	20		
					3.8	20
	21–22 kyr	3	40.1	16.2		
RC13-110	surface	1	32.3	17		
					1.5	10
	21–22 kyr	2	33.1	15.5		

[a]Also shown is a minimal difference estimate made by adding the calcite preserved standard error (5.8%) to the modern value, and subtracting it from the LGM value when calculating calcite flux (calcite accumulation rate/fraction calcite preserved).

[49] **Acknowledgments.** Thanks especially to the core curators at Oregon State University (June Padman and Bobbi Conard), Lamont Doherty Earth Observatory (Rusty Lotti-Bond), and the Ocean Drilling Program for their prompt and cheerful help in sampling. Mathieu Richaud aided in calcite analyses, and Mark Howland helped prepare several diagrams. Thanks are due to David Archer for providing us with his Muds model and for showing us how to use it. This research was partly supported by NSF grant OCE-0095617 and funds from the Northern Illinois University Graduate School (Loubere); the NASA Michigan Space Grant Consortium Seed Grant for summer, 2001 for ^{230}Th analyses at WHOI (Mekik); the French Ministere de l'Education Nationale, de la Recherche et de la Technologie, and a EURODOC grant from the Region Rhone-Alpes (Pichat).

References

Anderson, R., and A. Fleer (1982), Determination of natural actinides and plutonium in marine particulate material, *Anal. Chem.*, *54*, 1142–1147.

Andreason, D., and A. Ravelo (1997), Tropical Pacific Ocean thermocline depth reconstructions for the last glacial maximum, *Paleoceanography*, *12*, 395–414.

Archer, D. (1991), Equatorial Pacific calcite preservation cycles: Production or dissolution?, *Paleoceanography*, *6*, 561–571.

Archer, D. (1996), A data driven model of the global calcite lysocline, *Global Biogeochem. Cycles*, *10*(3), 511–526.

Archer, D., and E. Maier-Reimer (1994), Effect of deep-sea sedimentary calcite preservation on atmospheric CO2 concentration, *Nature*, *367*, 260–264.

Archer, D. E., J. L. Morford, and S. R. Emerson (2002), A model of suboxic sedimentary diagenesis suitable for automatic tuning and gridded global domains, *Global Biogeochem. Cycles*, *16*(1), 1017, doi:10.1029/2000GB001288.

Arrhenius, G. (1952), Sediment cores from the east Pacific, *Rep. Swed. Deep Sea Exped.*, *1947–1949*(5), 1–228.

Arrhenius, G. (1988), Rate of production, dissolution and accumulation of biogenic solids in the ocean, *Palaeogeogr. Palaeoclimatol. Palaeoecol.*, *67*, 119–146.

Bacon, M. P. (1984), Glacial to interglacial changes in carbonate and clay sedimentation in the Atlantic Ocean estimated from ^{230}Th measurements, *Isotope Geosci.*, *2*, 97–111.

Behrenfeld, M., and P. Falkowski (1997), Photosynthetic rates derived from satellite-based chlorophyll concentration, *Limnol. Oceanogr.*, *42*, 1–20.

Berelson, W., et al. (1997), Biogenic budgets of particle rain, benthic remineralization and sediment accumulation in the equatorial Pacific, *Deep Sea Res. Part II*, *44*, 2251–2281.

Berger, W. (1973), Deep-sea carbonate: Pleistocene dissolution cycles, *J. Foraminiferal Res.*, *3*, 187–195.

Berger, W., V. Smetacek, and G. Wefer (1989), Ocean productivity and paleoproductivity—An overview, in *Productivity of the Ocean: Present and Past*, edited by W. Berger et al., pp. 1–34, John Wiley, Hoboken, N. J.

Choi, M., R. Francois, K. Sims, M. Bacon, S. Brown-Leger, A. Fleer, L. Ball, D. Schneider, and S. Pichat (2001), Rapid determination of ^{230}Th and ^{231}Pa in seawater by desolvated-micronebulization inductively-coupled magnetic sector mass spectrometry, *Mar. Chem.*, *76*, 99–112.

Coale, K., et al. (1996), A massive phytoplankton bloom induced by an ecosystem-scale iron fertilization experiment in the equatorial Pacific Ocean, *Nature*, *383*, 495–501.

Dugdale, R., and F. Wilkerson (1998), Silicate regulation of new production in the equatorial Pacific upwelling, *Nature*, *391*, 270–273.

Dugdale, R., F. Wilkerson, and H. Minas (1995), The role of a silica pump in driving new production, *Deep Sea Res. Part I*, *42*, 697–719.

Farrell, J., and W. Prell (1989), Climatic change and CaCO3 preservation: An 800,000 year bathymetric reconstruction from the central equatorial Pacific Ocean, *Paleoceanography*, *4*, 447–466.

Farrell, J., et al. (1995), Glacial-interglacial changes in nutrient utilization in the equatorial Pacific Ocean, *Nature*, *377*, 514–517.

Francois, R., et al. (1990), Th-230 profiling in deep-sea sediments: High resolution records of flux and dissolution of carbonate in the equatorial Atlantic during the last 24,000 years, *Paleoceanography*, *5*(5), 761–787.

Francois, R., M. Frank, M. M. Rutgers van der Loeff, and M. P. Bacon (2004), ^{230}Th normalization: An essential tool for interpreting sedimentary fluxes during the late Quaternary, *Paleoceanography*, *19*, PA1018, doi:10.1029/2003PA000939.

Ganeshram, R., T. Pedersen, S. Calvert, and J. Murray (1995), Evidence from nitrogen isotopes for large changes in glacial-interglacial oceanic nutrient inventories, *Nature*, *376*, 755–758.

Ganeshram, R., et al. (2000), Glacial-interglacial variability in denitrification in the world's ocean: Causes and consequences, *Paleoceanography*, *15*, 361–376.

Henderson, G. M., et al. (1999), Global distribution of the 230-Th flux to ocean sediments constrained by GCM modeling, *Deep Sea Res. Part I*, *46*, 1861–1893.

Higgins, S., R. Anderson, F. Marcantonio, P. Schlosser, and M. Stute (2002), Sediment focusing creates 100-ka cycles in interplanetary dust accumulation on the Ontong-Java plateau, *Earth Planet. Sci. Lett.*, *203*, 383–397.

Honjo, S., D. Spencer, and J. Farrington (1982), Deep advective transport of lithogenic particles in the Panama Basin, *Science*, *216*, 516–518.

Jasper, J., et al. (1994), Photosynthetic fractionation of 13-C and concentrations of CO2 in the central equatorial Pacific during the last 225,000 years, *Paleoceanography*, *9*, 781–798.

Keil, R., et al. (1994a), Mineralogical and textural controls on the organic carbon composition of coastal sediments: Hydrodynamic separation using SPLITT fractionation, *Geochim. Cosmochim. Acta*, *58*, 879–893.

Keil, R., et al. (1994b), Sorptive preservation of labile organic matter in marine sediments, *Nature*, *370*, 549–552.

Koutavas, A., et al. (2002), El Niño-like pattern in ice age tropical Pacific sea surface temperature, *Science*, *297*, 226–230.

Loubere, P. (1999), A multiproxy reconstruction of biological productivity and oceanography in the eastern equatorial Pacific for the past 30,000 years, *Mar. Micropaleontol.*, *37*, 173–198.

Loubere, P. (2000), Marine control of biological production in the eastern equatorial Pacific, *Nature*, *406*, 497–500.

Loubere, P. (2001), Nutrient and oceanographic changes in the eastern equatorial Pacific from the last full glacial to the present, *Global Planet. Change*, *29*, 77–98.

Loubere, P. (2002), Remote vs. Local control of changes in eastern equatorial Pacific bioproductivity from the Last Glacial Maximum to the present, *Global Planet. Change*, *35*, 113–126.

Loubere, P., M. Fariduddin, and R. Murray (2003), Patterns of export production in the eastern equatorial Pacific over the past 130,000 years, *Paleoceanography*, *18*(2), 1028, doi:10.1029/2001PA000658.

Lyle, M., D. Murray, B. Finney, J. Dymond, J. Robbins, and K. Brookforce (1988), The record of late Pleistocene biogenic sedimentation in the eastern tropical Pacific Ocean, *Paleoceanography*, *3*, 39–59.

Lyle, M., et al. (1992a), Upwelling and productivity changes inferred from a temperature record in the central equatorial Pacific, *Nature*, *355*, 812–815.

Lyle, M., et al. (1992b), Paleoproductivity and carbon burial across the California current: The multitracers transect, 42 N, *Paleoceanography*, *7*, 215–272.

Lyle, M., A. Mix, and N. Pisias (2002), Patterns of $CaCO_3$ deposition in the eastern tropical Pacific Ocean for the last 150 kyr: Evidence for a southeast Pacific depositional spike during marine isotope stage (MIS) 2, *Paleoceanography*, *17*(2), 1013, doi:10.1029/2000PA000538.

Marcantonio, F., R. Anderson, S. Higgins, M. Stute, P. Schlosser, and P. Kubik (2001), Sediment focusing in the central equatorial Pacific Ocean, *Paleoceanography*, *16*(3), 260–267.

Martinson, D., N. Pisias, J. Hays, J. Imbrie, T. Moore, and N. Shackleton (1987), Age dating the orbital theory of the Ice Ages: Development of a high-resolution 0 to 300,000 year chronostratigraphy, *Quat. Res.*, *27*, 1–29.

Matsumoto, K., J. L. Sarmiento, and M. A. Brzezinski (2002), Silicic acid leakage from the Southern Ocean: A possible explanation for glacial atmospheric pCO_2, *Global Biogeochem. Cycles*, *16*(3), 1031, doi:10.1029/2001GB001442.

Mayer, L. (1994a), Relationships between mineral surfaces and organic carbon concentrations in soils and sediments, *Chem. Geol.*, *114*, 347–363.

Mayer, L. (1994b), Surface area control of organic matter accumulation in continental shelf sediments, *Geochim. Cosmochim. Acta*, *58*, 1271–1284.

Mekik, F. A., P. W. Loubere, and D. E. Archer (2002), Organic carbon flux and organic carbon to calcite flux ratio recorded in deep-sea carbonates: Demonstration and a new proxy, *Global Biogeochem. Cycles*, *16*(3), 1052, doi:10.1029/2001GB001634.

Mix, A., and A. Morey (1996), Climate feedback and Pleistocene variations in the Atlantic South Equatorial Current, in *The South Atlantic: Present and Past Circulation*, edited by G. Wefer et al., pp. 503–525, Springer-Verlag, New York.

Mix, A., J. Le, and N. Shackleton (1995a), Benthic foraminiferal stable isotope stratigraphy of site 846: 0–1.8 Ma, *Proc. Ocean Drill. Prog. Sci. Results*, *138*, 839–854.

Mix, A., N. Pisias, W. Rugh, J. Wilson, A. Morey, and T. Hagelberg (1995b), Benthic foraminifer stable isotope record from site 849 (0–5 Ma): Local and global climate changes, *Proc. Ocean Drill. Prog. Sci. Results*, *138*, 371–412.

Mix, A., A. Morey, N. Pisias, and S. Hostetler (1999), Foraminiferal faunal estimates of paleotemperature: Circumventing the no-analog problem yields cool ice age tropics, *Paleoceanography*, *14*, 350–359.

Murray, J., et al. (1994), Physical and biological controls on the carbon cycling in the equatorial Pacific, *Science*, *266*, 58–65.

NOAA (1994), World Ocean Atlas, vols. 2–4, U.S. Dept. of Commerce, Washington, D. C.

Paytan, A., M. Kastner, and F. Chavez (1996), Glacial to interglacial fluctuations in productivity in the equatorial Pacific as indicated by marine barite, *Science*, *274*, 1355–1357.

Pedersen, T. (1983), Increased productivity in the eastern equatorial Pacific during the last glacial maximum (19000 to 14000 Y. B. P.), *Geology*, *11*, 16–19.

Pedersen, T., B. Nielsen, and M. Pickering (1991), Timing of Late Quaternary productivity pulses in the Panama Basin and implications for atmospheric CO_2, *Paleoceanography*, *6*, 657–678.

Pisias, N., and A. Mix (1997), Spatial and temporal oceanographic variability of the eastern equatorial Pacific during the late Pleistocene: Evidence from radiolarian microfossils, *Paleoceanography*, *12*, 381–394.

Pisias, N., and D. Rea (1988), Late Pleistocene paleoclimatology of the central equatorial Pacific: Sea surface response to the southeast trade winds, *Paleoceanography*, *3*, 21–37.

Pisias, N., and Shipboard Scientific Party (1995), *Back Pocket Materials: Proceedings of the Ocean Drilling Program*, *Scientific Results*, vol. 138, 960 pp., Ocean Drill. Program, College Station, Tex.

Pisias, N., A. Mix, and R. Zahn (1990), Nonlinear response in the global climate system: Evidence from benthic oxygen isotope record in core RC13-110, *Paleoceanography*, *5*, 147–160.

Rea, D., N. Pisias, and T. Newberry (1991), Late Pleistocene paleoclimatology of the central equatorial Pacific: Flux patterns of biogenic sediments, *Paleoceanography*, *6*, 227–244.

Rodgers, K. B., B. Blanke, G. Madec, O. Aumont, P. Ciais, and J.-C. Dutay (2003), Extratropical sources of equatorial Pacific upwelling in an OGCM, *Geophys. Res. Lett.*, *30*(2), 1084, doi:10.1029/2002GL016003.

Sanyal, A., et al. (1997), Changes in pH in the eastern equatorial Pacific across the stage 5–6 boundary based on boron isotopes in foraminifera, *Global Biogeochem. Cycles*, *11*, 125–133.

Sarnthein, M., et al. (1988), Global variations of surface ocean productivity in low and mid latitudes: Influence on CO2 reservoirs of the deep ocean and the atmosphere during the last 21,000 years, *Paleoceanography*, *3*, 361–399.

Schrader, H., and R. Sorknes (1990), Spatial and temporal variation of Peruvian coastal upwelling during the latest Quaternary, *Proc. Ocean Drill. Program Sci. Results*, *112*, 391–406.

Smith, W., and D. Sandwell (1997), Global sea floor topography from satellite altimetry and ship depth soundings, *Science*, *277*, 1957–1962.

Snoeckx, H., and D. Rea (1994), Late Quaternary CaCO3 stratigraphy of the eastern equatorial Pacific, *Paleoceanography*, *9*, 341–351.

Snoeckx, H., and D. Rea (1995), Data report: CaCO3 content and bulk density of Leg 138 site-survey piston cores, *Proc. Ocean Drill. Prog. Sci. Results*, *138*, 885–894.

Spero, H., and D. Lea (2002), The cause of carbon isotope maximum events on glacial terminations, *Science*, *296*, 522–525.

Stephens, M., and D. Kadko (1997), Glacial-Holocene calcium carbonate dissolution at the central equatorial Pacific seafloor, *Paleoceanography*, *12*, 797–804.

Suman, D., and M. Bacon (1989), Variations in Holocene sedimentation in the North American Basin determined from 230-Th measurements, *Deep Sea Res.*, *36*, 869–878.

Takahashi, T., et al. (2002), Global sea-air CO_2 flux based on climatological surface ocean pCO_2 and seasonal biological and temperature effects, *Deep Sea Res. Part II*, *49*, 1601–1622.

Toggweiler, J., D. Dixon, and W. Broecker (1991), The Peru upwelling and the ventilation of the South Pacific thermocline, *J. Geophys. Res.*, *96*, 20,467–20,497.

Van Andel, T. (1973), Texture and dispersal of sediments in the Panama Basin, *J. Geol.*, *81*, 434–457.

Verardo, D., P. Froelich, and A. McIntyre (1990), Determination of organic carbon and nitrogen in marine sediments using the Carlo Erba NA-1500 Analyzer, *Deep Sea Res.*, *37*, 157–165.

Weber, M., M. Wiedicke, and V. Riech (1995), Carbonate preservation history in the Peru Basin: Paleoceanographic implications, *Paleoceanography*, *10*(4), 775–800.

Wefer, G., et al. (1990), Stratigraphy and sedimentation rates from oxygen isotope composition, organic carbon content, and grain-size distribution at the Peru upwelling region: Holes 680B and 686B, *Proc. Ocean Drill. Program Sci. Results*, *112*, 355–367.

Wilkerson, F., and R. Dugdale (1996), Silicate versus nitrate limitation in the equatorial Pacific estimated from satellite-derived sea-surface temperatures, *Adv. Space Res.*, *18*(7), 81–89.

Yu, E.-F., R. Francois, M. Bacon, S. Honjo, A. Fleer, S. Manganini, M. Rutgers van der Loeff, and V. Ittekot (2001), Trapping efficiency of bottom-tethered sediment traps estimated from the intercepted fluxes of 230-Th and 231-Pa, *Deep Sea Res. Part I*, *48*, 865–889.

R. Francois, Department of Marine Chemistry and Geochemistry, Woods Hole Oceanographic Institution, Woods Hole, MA 02543, USA. (rfrancois@whoi.edu)

P. Loubere, Department of Geology and Environmental Geosciences, Northern Illinois University, DeKalb, IL 60115, USA. (paul@geol.niu.edu)

F. Mekik, Department of Geology, Grand Valley State University, Allendale, MI 49401, USA. (mekikf@gvsu.edu)

S. Pichat, Department of Earth Sciences, Oxford University, Park Road, Oxford OX 1 3PR, UK.

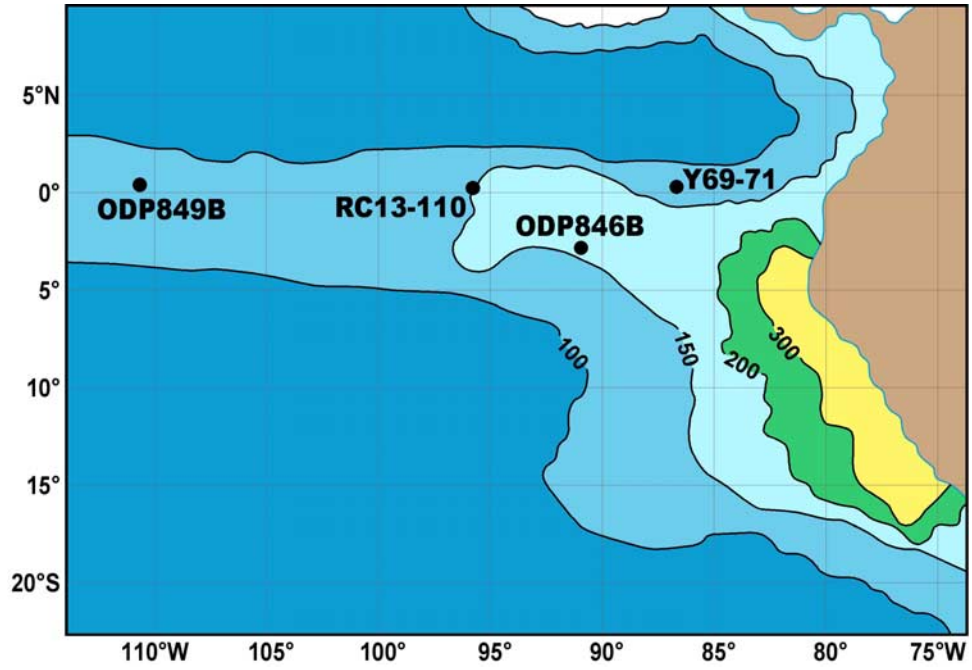

Figure 1. Core locations in the eastern equatorial Pacific. Color gradient represents surface ocean biological productivity after the standard model of *Behrensfeld and Falkowski* [1997]. Contours in gC m^{-2} yr^{-1}.

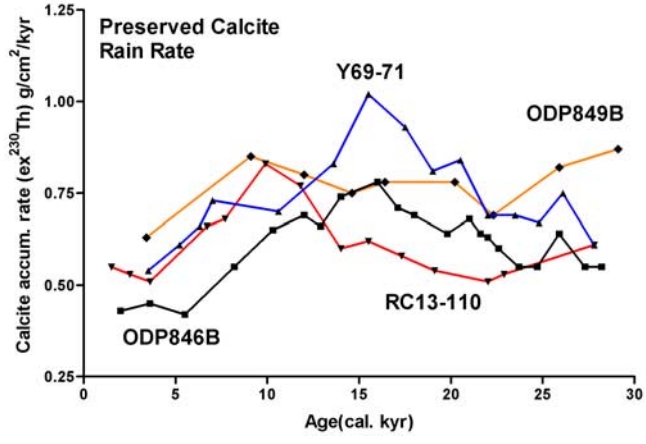

Figure 4. Preserved calcite rain rates for the four cores based on method B in the text (ex^{230}Th normalization). Data in Table 3.

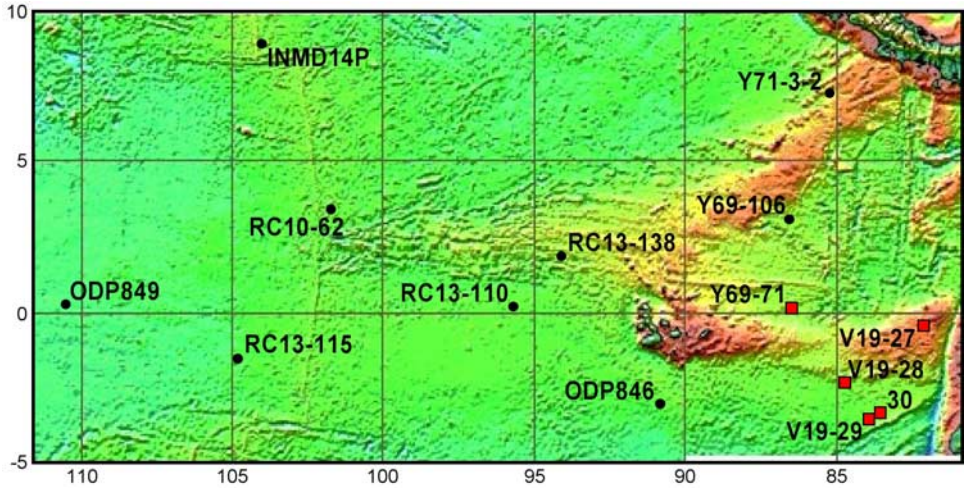

Figure 7. Core locations for this study and *Lyle et al.* [2002] used for calcite accumulation rate determinations, plotted on bathymetry from *Smith and Sandwell* [1997]. Locations marked by squares are those showing elevated LGM preserved calcite mass accumulation rates.

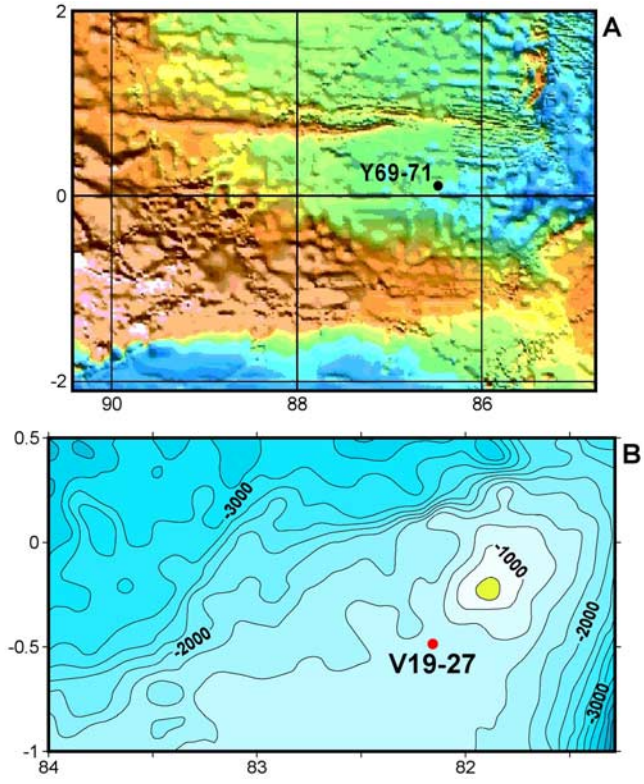

Figure 8. (a) Location of Y69-71 on multibeam bathymetry from the RIDGE Web site (http://ocean-ridge.ldeo.columbia.edu/general/html/RMBS-intro.html; http://ocean-ridge.ldeo.columbia.edu/database/html/home.html). (b) Location of V19-27 on bathymetry from *Smith and Sandwell* [1997]; see http://topex.ucsd.edu/marine_topo/mar_topo.html.

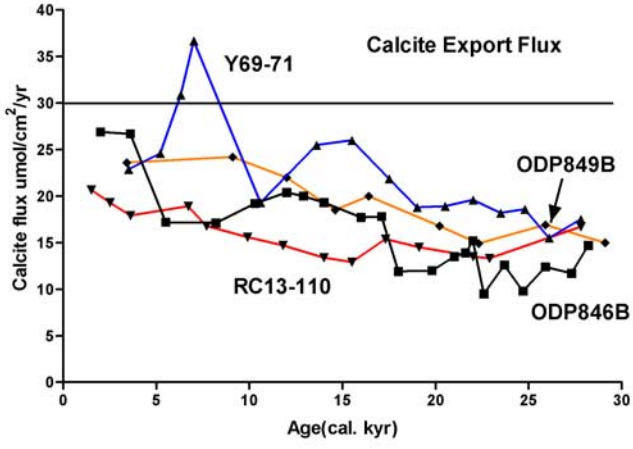

Figure 11. Calcite export flux calculated for the four cores found by dividing the ex^{230}Th accumulation rates by fraction calcite preserved. Note that umol cm^{-2} yr^{-1} = 10 × g cm^{-2} kyr^{-1}.